One-Dimensional Fast Migration of Vacancy Clusters in Metals

Yoshitaka Matsukawa, *et al.*

Science **318**, 959 (2007);
DOI: 10.1126/science.1148336

where N_{dk} is the total number of double kinks. By an extension of Eq. 4, D is approximated as

$$D \approx a^2 \left\langle \left[\frac{2(n_f - n_b)}{L}\right]^2 \right\rangle D_k = \frac{2a^2}{L} c_k D_k \propto N^{-0.5} c_k D_k \quad (7)$$

where L is the loop-line length and D_k is the kink diffusivity. Even when $N_{dk} < 1$, the identical result is obtained (*17*). The power of N reduces for extremely small N because the attractive force is applied on two adjacent kinks of opposite signs (*2*), accelerating the motion of both kinks so that they coalesce. This satisfies the dependence of D_0 on N, as obtained in the present study. The temperature dependence of D is expressed by the term $c_k D_k$ in Eq. 7. D_k is controlled by the dragged impurity atmosphere surrounding the dislocation. The dragging stress applied onto a dislocation by the atmosphere is generally proportional to the velocity of the dislocation, when the atmosphere can promptly follow the dislocation motion (*1*, *26*, *27*). If we set the proportionality factor to be B (*27*), D_k can be approximated with the use of Einstein's relation (*22*)

$$D_k \approx \frac{kT}{abB} \approx \frac{\alpha D_c (kT)^2}{c_0} \quad (8)$$

where b is the absolute value of **b**, α is the constant, c_0 is the concentration of dragged impurities in the matrix, and D_c [$= D_{c,0} \exp(-E_c/kT)$, where E_c is the activation energy for the migration of dragged impurities] is the diffusivity of the impurity atoms that compose the atmosphere (*24*). Here, other effects influencing D_k—such as phonon dragging, electron dragging, and Peierls potential of the second kind (*1*, *28*)—are neglected. From Eqs. 5, 7, and 8, the apparent activation energy for the diffusion of a loop is expressed as

$$E \equiv -\frac{d \ln D}{d(1/kT)} = E_k + E_c + \frac{3}{2} kT \quad (9)$$

In contrast, if the atmosphere dragging does not occur and the phonon dragging due to the phonon wind (*28*) is dominant, D_k for this "naked" loop becomes constant above the Debye temperature. This yields $E = E_k - \frac{1}{2}kT$. In general, the addition of solutes into pure Fe changes the shear modulus only slightly (*29*); therefore, their atmosphere will not effectively influence the E_k value. Thus, E increases by $E_c + 2kT$ when the loop drags the atmosphere. The most probable elements composing the dragged atmosphere of all the impurity elements are C or N. We do not know the precise values of E_c for C or N around the dislocation. However, if we adopt E_c values for C or N ($E_c = 0.83$ eV for C, $E_c = 0.80$ eV for N) (*19*), both the E_k value and the E value for "naked" loops become ~0.4 eV.

Using in situ TEM, we have shown that nanometer-sized dislocation loops can undergo 1D diffusion even in the absence of stresses that are effective in driving loops. These findings are relevant for the prediction of the lifetime of radiation-resistant materials for nuclear fission and energy systems in which the microstructures are controlled by the motion of loops formed upon high-energy particle irradiation. In addition, this study opens up a pathway for further experimental investigation of the unresolved dynamics of extremely small self-interstitial atom complexes.

References and Notes

1. J. P. Hirth, J. Lothe, *Theory of Dislocations* (Wiley, New York, 1982).
2. A. Seeger, P. Schiller, in *Physical Acoustics*, W. P. Mason, Ed. (Academic Press, New York, 1966), vol. 3, part A, pp. 361–512.
3. B. D. Wirth, G. R. Odette, D. Maroudas, G. E. Lucas, *J. Nucl. Mater.* **276**, 33 (2000).
4. N. Soneda, T. D. De la Rubia, *Philos. Mag. A* **81**, 331 (2001).
5. J. Marian *et al.*, *Phys. Rev. B* **65**, 144102 (2002).
6. Y. N. Osetsky, D. J. Bacon, A. Serra, B. N. Singh, S. I. Golubov, *Philos. Mag.* **83**, 61 (2003).
7. D. A. Terentyev, L. Malerba, M. Hou, *Phys. Rev. B* **75**, 104108 (2007).
8. A. V. Barashev, Yu. N. Osetsky, D. J. Bacon, *Philos. Mag. A* **80**, 2709 (2000).
9. S. L. Dudarev, *Phys. Rev. B* **65**, 224105 (2002).
10. K. Ohsawa, E. Kuramoto, *Phys. Rev. B* **72**, 054105 (2005).
11. H. Trinkaus, B. N. Singh, S. I. Golubov, *J. Nucl. Mater.* **283–287**, 89 (2000).
12. D. Walgraef, N. M. Ghoniem, *Phys. Rev. B* **67**, 064103 (2003).
13. J. R. Manning, *Diffusion Kinetics for Atoms in Crystals* (Van Nostrand, Princeton, NJ, 1968).
14. M. Kiritani, *J. Nucl. Mater.* **251**, 237 (1997).
15. H. Abe, N. Sekimura, Y. Yang, *J. Nucl. Mater.* **323**, 220 (2003).
16. K. Arakawa, M. Hatanaka, E. Kuramoto, K. Ono, H. Mori, *Phys. Rev. Lett.* **96**, 125506 (2006).
17. See supporting material on *Science* Online.
18. A. H. Cottrell, *Reports on the Strength of Solids* (Physical Society, London, 1948), p. 30.
19. A. E. Lord Jr., D. N. Beshers, *Acta Metall.* **14**, 1659 (1966).
20. N. Louat, *Proc. Phys. Soc. B* **69**, 459 (1956).
21. J. Th. M. de Hosson, *Solid State Commun.* **17**, 747 (1975).
22. S. Chandrasekhar, *Rev. Mod. Phys.* **15**, 1 (1943).
23. G. A. Cottrell, S. L. Dudarev, R. A. Forrest, *J. Nucl. Mater.* **325**, 195 (2004).
24. T. Heumann, *Diffusion in Metallen* (Springer, Berlin, 1992).
25. G. Schoeck, in *Dislocations in Solids*, F. R. N. Nabarro, Ed. (North-Holland, Amsterdam, 1980), vol. 3, pp. 63–163.
26. H. Yoshinaga, S. Morozumi, *Philos. Mag.* **23**, 1367 (1971).
27. A. H. Cottrell, M. A. Jaswon, *Proc. R. Soc. London Ser. A* **199**, 104 (1949).
28. V. I. Alshits, V. L. Indenbom, in *Dislocations in Solids*, F. R. N. Nabarro, Ed. (North Holland, Amsterdam, 1986), vol. 7, pp. 43–111.
29. G. R. Speich, A. J. Schwoeble, W. C. Leslie, *Metall. Trans.* **3**, 2031 (1972).

30. We thank Nippon Mining & Metal Co. Ltd. for the careful heat treatment of the experimental specimens. Supported by the Ministry of Education, Sports, Culture, Science and Technology of Japan (Grant-in-Aid for Scientific Research 17760530) and by Priority Assistance for the Formation of Worldwide Renowned Centers of Research—The Global COE Program (Project: Center of Excellence for Advanced Structural and Functional Materials Design) from the same ministry.

Supporting Online Material

www.sciencemag.org/cgi/content/full/318/5852/956/DC1
Materials and Methods
SOM Text
Figs. S1 to S4
Table S1
References
Movies S1 and S2

18 May 2007; accepted 3 October 2007
10.1126/science.1145386

One-Dimensional Fast Migration of Vacancy Clusters in Metals

Yoshitaka Matsukawa[1,2]*† and Steven J. Zinkle[1]

The migration of point defects, for example, crystal lattice vacancies and self-interstitial atoms (SIAs), typically occurs through three-dimensional random walk in crystalline solids. However, when vacancies and SIAs agglomerate to form planar clusters, the migration mode may change. We observed nanometer-sized clusters of vacancies exhibiting one-dimensional (1D) fast migration. The 1D migration transported a vacancy cluster containing several hundred vacancies with a mobility higher than that of a single vacancy random walk and a mobility comparable to a single SIA random walk. Moreover, we found that the 1D migration may be a key physical mechanism for self-organization of nanometer-sized sessile vacancy cluster (stacking fault tetrahedron) arrays. Harnessing this 1D migration mode may enable new control of defect microstructures such as effective defect removal and introduction of ordered nanostructures in materials, including semiconductors.

The one-dimensional (1D) fast migration of nanometer-sized defect clusters is currently of particular interest in nuclear materials research (*1*). Recent molecular dynamics (MD) simulations have indicated that nanometer-sized, sessile clusters of vacancies and glissile clusters of self-interstitial atoms (SIAs) are produced together in collision cascades during energetic ion and neutron irradiation (*2*). In face-centered cubic (fcc) metals, sessile vacancy clusters often form stacking fault tetrahedra (SFTs) having 3D pyramidal structure. The configuration of the glissile SIA clusters is a 2D platelet, 1/2<110>{110} prismatic perfect dislocation loop. Sufficiently small SIA clusters can exhibit 1D fast migration (*3*–*8*), which transports the entire cluster contain-

ing several tens of SIAs with a mobility comparable to that of a single SIA (*4*). This anisotropic migration of SIA clusters is currently considered to have a noticeable impact on the evolution of a material's neutron-irradiation damage microstructure, which determines the material's lifetime in nuclear reactor environments (*1*, *9*).

Although SIA clusters form a dislocation loop, the 1D migration may involve a cooperative atomic diffusion mechanism not described by conventional dislocation theory. Because the line senses of dislocation segments facing each other in a loop are always opposite, it is impossible to glide the whole loop in the same direction simultaneously under shear stress, as shown in fig. S1. In theory, it is possible to induce glide of the entire loop in the same direction by pushing the atoms in the prismatic column from one side. This type of motion, which is traditionally called prismatic punching, proposed by Seitz (*10*), can be induced in specific situations, such as indentation. However, the loop's 1D motion observed in irradiated metals is not one way but reciprocates back and forth, as reported by several researchers (*11*–*14*). Therefore, prismatic punching does not appear to be a viable mechanism. A widely accepted mechanism for the 1D migration has its basis in thermally activated dense fluctuation of its constituent elements, "crowdions," in the dense packed <110> atomic direction along their Burgers vector in the case of fcc metals (*4*), as shown schematically in Figs. 1 and 2. Figure 2 schematically shows the relationship between the loop 1D migration direction, geometry of the loop, and bundled crowdions. Because the 1D migration is induced by collective motion of numerous neighboring crowdions in the loop, this phenomenon is substantial only when the loop size is small: MD simulations have indicated that only nanometer-sized SIA loops exhibit 1D migration (*4*). A previously proposed alternative account for the 1D motion within the scope of dislocation theory is that the loop motion is induced by the thermally activated formation and propagation of a double kink on the loop, which is expressed by a (dislocation) line tension model (*5*, *15*), as shown in fig. S2. However, in 1D motion all of the crowdions inside the prismatic cylinder must be transported, whereas the line tension model only describes the motion of crowdions on the dislocation line. In MD simulations, inner crowdions are often observed to move before the crowdions on the loop perimeter (as schematically shown in fig. S2F): The motion of whole loop is led by the inner crowdions (*16*).

A fundamental question is whether the 1D migration is also possible for vacancy-type prismatic dislocation loops. Osetsky *et al.* examined the possibility of 1D migration for vacancy loops in both body-centered cubic (bcc) and fcc metals by using MD simulations (*17*). They predicted 1D migration of small vacancy loops in bcc iron but not in fcc copper. The prismatic vacancy loop in copper immediately became sessile by developing stacking faults from the loop edges within a picosecond. They attributed the absence of 1D migration in fcc copper to its low stacking fault energy. To date, there have been no observations of 1D migration of vacancy clusters, whereas several experimental studies have reported 1D migration of SIA clusters (*11*–*14*). Thus, based on the MD results, the existing consensus is that the 1D migration of vacancy clusters is not possible, especially in fcc metals (*1*).

In the present study, vacancy loops were introduced into 99.9975% pure fcc gold through plastic deformation or quenching and then examined in a nominally stress-free condition. The stacking fault energy of gold (32 mJ/m^2) is even lower than that for copper (45 mJ/m^2), which would promote conversion of dislocation loops to SFTs even more strongly in gold than in copper (*18*). Therefore, 1D migration of vacancy clusters is not expected in gold. A very high density of vacancy clusters is produced by plastic deformation in ductile metal thin foils having a specific geometry (*19*). Although the majority of vacancy clusters produced by plastic deformation at room temperature in gold are SFTs (*19*), a few vacancy-type dislocation loops are also produced. Those dislocation loops exhibited 1D oscillating motion, inconsistent with the reported MD simulation results. Figure 3 and movie S1 show an example of the observed behavior at room temperature. A small dislocation loop (diameter about 2 nm, ~174 vacancies) glided intermittently back and forth between two SFTs at an oblique angle along the projection of the <110> direction (oscillating distance of 1 to 2 nm). The loop position changed frame by frame (frame rate of 30 frames/s) for about 4 min and then suddenly transformed to an SFT within a few video frames (<0.1 s). Because SFTs are vacancy-type defects in fcc structures (*20*), Fig. 3 provides evidence that nanometer-sized vacancy loops can exhibit 1D migration. The vacancy loop transformed into an SFT at an intermediate position between two preexisting SFTs, presumably because the stress field on the loop from the two SFTs is balanced at the intermediate position. As a result, a well-aligned SFT array consisting of three SFTs was obtained.

There are many reports showing ordered arrays of nanometer-sized SFTs created through high-energy particle irradiation such as neutron irradiation and ion bombardment (*21*–*23*). Because SFTs are sessile, it has been believed that the self-organized microstructure is created by glissile SIA clusters exhibiting 1D migration; vacancy clusters that are geometrically aligned along close-packed <110> directions in fcc crystals would be preferentially shielded from annihilation by the 1D migrating SIA clusters. However, the present dynamic observation (Fig. 3) suggests that spatial self-organization of sessile SFTs can be achieved through the 1D migration (and conversion to SFTs) of glissile vacancy loops, without the necessity of 1D migration of SIA clusters. Fig. S3 shows previously proposed models of loop-SFT conversion (*24*), and fig. S4 shows the crystallography of various potential loop geometries.

Figure 4 and movies S2 and S3 show the 1D migration of a vacancy loop introduced into gold

[1]Materials Science and Technology Division, Oak Ridge National Laboratory (ORNL), Post Office Box 2008, TN 37831–6138, USA. [2]Center for Materials Processing, University of Tennessee, Knoxville, TN 37996–0750, USA.

*Present address: Department of Materials Science and Engineering, University of Illinois at Urbana-Champaign, Materials Science and Engineering Building 408A, 1304 West Green Street, Urbana, IL 61801, USA.

†To whom correspondence should be addressed. E-mail: ym2@uiuc.edu

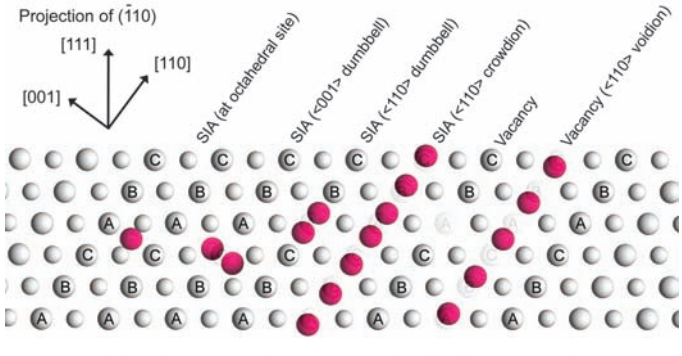

Fig. 1. Various atom configurations of SIAs and vacancies projected on $(\bar{1}01)$: small atoms represent atoms on a plane ¼$[\bar{1}01]$ below the large atoms. In the fcc structure, single SIAs are preferentially located at octahedral sites denoted as (1/2, 1/2, 1/2) on the basis of atomic volume considerations; however, it is energetically more favorable to be arranged in a <001> dumbbell structure. The crowdion distributes the localized displacement of the SIA along the <110> close-packed atom direction. Subtracting an atom, i.e., introduction of a vacancy, may create a delocalized dilute atom configuration complementary to the <110> crowdion (<110> voidion). Note that this configuration never occurs for single vacancies.

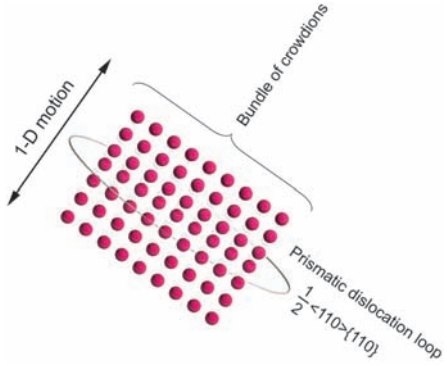

Fig. 2. Schematic sketch of the 1D migration of the SIA-type 1/2<110>{110} dislocation loop and its atomic structure.

by quenching that introduces only vacancies. The transmission electron microscopy (TEM) observation was carried out at 113 K. The vacancy loop (diameter about 3.5 nm; ~534 vacancies) exhibited oscillating 1D migration for about 6 min, whereas single vacancies were immobile below ~300 K in gold (*25*). The loop wiggled intermittently, back and forth, along a straight dislocation with a wide variety of migration distances for each oscillation. The maximum observed migration distance per oscillation (within two video frames, i.e., 66 ms) was 15 nm, which corresponds to 52 times the {110} interplanar distance in gold. In general, the number of atomistic jumps per second in a thermally activated process is expressed as $\nu = \nu_0 \exp(S/k)\exp(-E_m/kT)$, where ν_0 is the lattice vibration frequency, k is the Boltzmann constant, S is entropy, and T is absolute temperature. We assume $\exp(S/k) = 1$ for the sake of simplicity. The migration energies of single vacancies and single SIAs in gold are $E_m = 0.85$ eV and $E_m = 0.19$ eV, respectively (*26*). With $\nu_0 = 10^{13}$ s^{-1}, ν at 113 K is 1.3×10^{-25} s^{-1} for single vacancies and 3.4×10^{4} s^{-1} for single SIAs. The maximum observed migration distance of the vacancy loop (15 nm) corresponds to $\nu = 789$ s^{-1}, which gives E_v of 0.22 to about 0.23 eV as the effective migration energy for the vacancy loop 1D motion (*27*). This effective migration energy for the 1D glissile vacancy loop is much less than that for single vacancies. This suggests that the mobility of nanometer-sized dislocation loops via 1D migration is independent of the mobility of the constituent point defects, that is, vacancies in this case.

The diffraction contrast images of the vacancy loops observed in the present study are quite unusual as a dislocation loop image. Seen from the <110> direction, the loop is in an edge-on view, i.e., visible as a line segment (*28*). However, the loop image in Fig. 4 is oval in shape, elongated in the 1D glide direction. The loop image in Fig. 3 is also oval in shape. This may be an artifact due to the high velocity of 1D motion. MD simulations (obtained for SIA loops) have indicated that the loop's oscillation is essentially a sub-picosecond–time scale event (*4*). Such high-speed motion cannot be captured by the present video-recording system, whose time resolution is 33 ms. Instead, a composite image of the loop's motion during ~33 ms is recorded on a single video frame. Note that the loop image remained the same even after the motion became undetectable in Fig. 4. This may be an indication that the loop was still moving one-dimensionally with a very short oscillating distance and high frequency, even after the large motion detectable by the present dynamic TEM observation disappeared.

The size of the vacancy loops observed in the present TEM study (2 to 3.5 nm) is much larger than the loop examined in the 1999 MD simulation (up to 50 vacancies; <1 nm). On the basis of the results on SIA loops obtained through MD simulations, larger loops are less mobile than small loops: The critical size above which the predicted mobility is practically zero is ~100 SIAs (~1.3 nm) in copper and ~300 SIAs (~2.4 nm) in iron (*4*). However, in TEM experiments, much larger SIA loops exhibit 1D migration above 450 K: The critical size in iron may be as large as 20 to ~30 nm (*11*). The present experimental results were obtained in a TEM operated at 200 keV, which is well below the critical voltage to introduce Frenkel pairs (vacancy and an SIA) into gold. The critical electron energy for Frenkel pair creation is ~2 MeV because of the large mass of gold atoms. The temperature increase by the 200-keV electron irradiation is negligible because the specimen was thin (<50 nm) and the electron beam diameter was less than 2 μm, which gives less than a few tens of Kelvin local temperature increase for the electron beam fluxes used in the present study (*29*).

Although vacancy loops cannot have crowdions, we speculate that they may develop an analogous (dilute) atom configuration similar to crowdions (we tentatively call this dilute-packed <110> atomic row "voidions"), as shown in Fig. 1. Such a configuration does not occur for single vacancies; however, in the form of a 1/2<110>{110} prismatic loop, numerous vacancies are neighboring on a {110} plane, potentially favoring this cooperative voidion configuration.

An unresolved question is whether the 1D migration of SIA and vacancy clusters can be effectively harnessed to enable directed assembly of technologically useful nanoscale architectures. The formation of a linear array of SFTs in Fig. 3 implies that it may be possible to create unique nanoscale ordered defect microstructures by particle irradiation. The very high mobility of the 1D glide vacancy clusters may also provide a hint regarding efficient defect removal from not only metals but also semiconductor materials, whose defect clustering behavior is essentially the same as fcc metals because of their similar crystal structures, as well as introduction of nanoscale ordered structures.

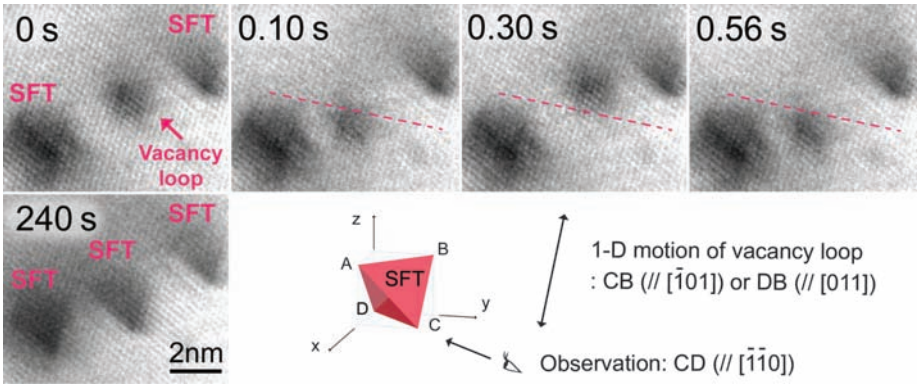

Fig. 3. Sequence of snapshots showing the 1D oscillating motion of a vacancy loop and eventual transformation to an SFT (after 240 s) in deformed gold at room temperature.

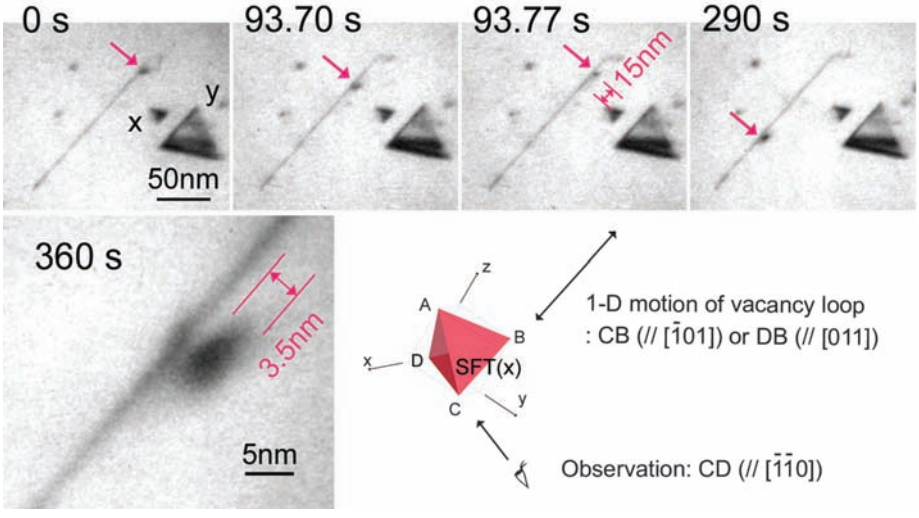

Fig. 4. Sequence of snapshots showing the 1D oscillating migration of a vacancy loop in quenched gold at 113 K. The spatial dimension shown in the frame of 93.77 s is the jump distance from the previous observed loop position at 93.70 s. Two types of crystallographically equivalent SFTs (marked by x and y) are involved in the figure.

References and Notes

1. B. N. Singh, in *Encyclopedia of Materials: Science and Technology*, K. H. J. Buschow *et al.*, Eds. (Elsevier, New York, 2001), pp. 7957–7972.

2. Yu. N. Osetsky, D. J. Bacon, *Nucl. Instrum. Methods Phys. Res. B* **180**, 85 (2001).
3. A. J. E. Foreman, C. A. English, W. J. Phythian, *Philos. Mag. A* **66**, 655 (1992).
4. Yu. N. Osetsky, D. J. Bacon, A. Serra, B. N. Singh, S. I. Golubov, *Philos. Mag.* **83**, 61 (2003).
5. J. Marian *et al.*, *Phys. Rev. B* **65**, 144102 (2002).
6. E. Kuramoto, *J. Nucl. Mater.* **276**, 143 (2000).
7. B. D. Wirth, G. R. Odette, D. Maroudas, G. E. Lucas, *J. Nucl. Mater.* **276**, 33 (2000).
8. S. L. Dudarev, *Philos. Mag.* **83**, 3577 (2003).
9. H. Trinkaus, B. N. Singh, A. J. E. Foreman, *J. Nucl. Mater.* **206**, 200 (1993).
10. F. Seitz, *Phys. Rev.* **79**, 723 (1950).
11. K. Arakawa, M. Hatanaka, E. Kuramoto, K. Ono, H. Mori, *Phys. Rev. Lett.* **96**, 125506 (2006).
12. M. Kiritani, *J. Nucl. Mater.* **251**, 237 (1997).
13. T. Hayashi, K. Fukumoto, H. Matsui, *J. Nucl. Mater.* **307–311**, 993 (2002).
14. H. Abe, N. Sekimura, Y. Yang, *J. Nucl. Mater.* **323**, 220 (2003).
15. K. Ohsawa, E. Kuramoto, *Phys. Rev. B* **72**, 054105 (2005).
16. The crowdions located at the loop center have a smaller energy barrier for motion than that of the crowdions located on the loop perimeter (*4*). This is because the most stable configuration for single SIAs is the dumbbell: The crowdions on the loop perimeter are more likely to transform to dumbbell configuration. Conversely, Marian (*5*) claimed that crowdion jumps are more likely to occur at the loop perimeter. This is because the interatomic potential used by Marian incorrectly predicts the crowdion configuration to be more stable than the dumbbell configuration.
17. Yu. N. Osetsky, D. J. Bacon, A. Serra, *Philos. Mag. Lett.* **79**, 273 (1999).
18. J. P. Hirth, J. Lothe, *Theory of Dislocations* (McGraw-Hill, New York, ed. 2, 1982).
19. M. Kiritani *et al.*, *Philos. Mag. Lett.* **79**, 797 (1999).
20. S. Kojima *et al.*, *Philos. Mag. A* **59**, 519 (1989).
21. N. M. Ghoniem, D. Walgraef, S. J. Zinkle, *J. Computer-Aided Mater. Des.* **8**, 1 (2002).
22. A. Seeger, N. Y. Jin, F. Phillip, M. Zaiser, *Ultramicroscopy* **39**, 342 (1991).
23. C. Tölg, P. Hähner, M. Zaiser, W. Frank, *Appl. Phys. A* **58**, 3 (1994).
24. D. Kuhlmann-Wilsdorf, *Acta Metall.* **13**, 257 (1965).
25. J. E. Bauerle, J. S. Koehler, *Phys. Rev.* **107**, 1493 (1957).
26. M. Kiritani, *J. Phys. Soc. Jpn.* **40**, 1035 (1976).
27. We did not regard the loop migration of 15 nm as a ballistic jump because of the following context. The 1D migration of dislocation loop is a result of collective motion of numerous atoms whose elementary jump length is d_{110}, the interplanar distance between (110) planes. Although the vacancy loop migrated ballistically 15 nm within a few video frames, it seems reasonable to assume that this migration consists of several hundred jumps of a few hundred atoms in the same direction, involving thermally activated atomic jumps in the reverse direction on an atomic scale.
28. The loop shape (triangle or circular) is unidentifiable in the edge-on view.
29. S. B. Fisher, *Radiat. Eff.* **5**, 239 (1970).

30. This research was sponsored by the Office of Fusion Energy Sciences, U.S. Department of Energy. The microscope facility within the SHaRE (Shared Research Equipment User Facility) Collaborative Research Center at ORNL was supported by the Division of Scientific User Facilities, Office of Basic Energy Science. We are grateful to Y. N. Osetsky, S. I. Golubov, B. N. Singh, and P. J. Kamenski for valuable comments.

Supporting Online Material

www.sciencemag.org/cgi/content/full/318/5852/959/DC1
Materials and Methods
SOM Text
Figs. S1 to S4
Movies S1 to S3

25 July 2007; accepted 3 October 2007
10.1126/science.1148336

Widespread Morning Drizzle on Titan

Máté Ádámkovics,[1,2]* Michael H. Wong,[1] Conor Laver,[1] Imke de Pater[1,2]

Precipitation is expected in Titan's atmosphere, yet it has not been directly observed, and the geographical regions where rain occurs are unknown. Here we present near-infrared spectra from the Very Large Telescope and W. M. Keck Observatories that reveal an enhancement of opacity in Titan's troposphere on the morning side of the leading hemisphere. Retrieved extinction profiles are consistent with condensed methane in clouds at an altitude near 30 kilometers and concomitant methane drizzle below. The moisture encompasses the equatorial region over Titan's brightest continent, Xanadu. Diurnal temperature gradients that cause variations in methane relative humidity, winds, and topography may each be a contributing factor to the condensation mechanism. The clouds and precipitation are optically thin at 2.0 micrometers, and models of "subvisible" clouds suggest that the droplets are 0.1 millimeter or larger.

A zoo of clouds is scattered across Saturn's largest moon, Titan, including convective clouds near the south pole (*1*, *2*), geographically controlled clouds at 40°S latitude (*3*), and a large cloud of ethane near the north pole (*4*). These and other types of clouds have been predicted with the use of combinations of chemical, microphysical, and general circulation models (*5*, *6*). Analysis of the methane relative humidity profile at the Huygens probe entry site suggests that there is a solid-methane cloud from 20 to 30 km altitude and a light drizzle of methane that wets the surface (*7*). However, the fluvial channels seen at the landing site (*8*) are due to heavier rainfall (*9*), which may occur during intense storms that are predicted by dynamical models (*10*). Conditions in the lower troposphere are best constrained where the Huygens probe landed, yet a single weather station cannot characterize Titan's meteorology on a planetwide scale. If widespread, methane condensation could be the dominant pathway for returning methane to the surface and closing the methane cycle.

Because the near-infrared aerosol opacity τ in Titan's atmosphere is low ($\tau = 0.2$ at 2 μm), light can penetrate to the surface at wavelengths where methane absorption is negligible (*11*). Radiative transfer (RT) models of Titan's spectra have been used to probe the heights of cloud tops and the aerosol vertical structure (*1*, *2*, *12*, *13*). One of the main challenges in accurately retrieving altitudes with these models is that the contribution function for a particular wavelength is dependent on the vertical distribution of aerosol. Variations in surface reflectivity can also be masked by near-surface atmospheric opacity. One way to break these degeneracies is to simultaneously analyze spectra taken along different paths through the atmosphere. Spatially resolved spectra from a new class of instruments, such as the OH-Suppressing InfraRed Imaging Spectrograph (OSIRIS) (*14*) at the W. M. Keck Observatory or the Spectrograph for INtegral Field Observations in the Near Infrared (SINFONI) (*15*) at the Very Large Telescope (VLT), are an ideal source of data for such an analysis. These instruments may be used to create a global picture of Titan's lower atmosphere and surface.

During our campaign to monitor the seasonal changes in the global distribution of Titan's aerosol, we observed Titan on 28 February 2005 universal time (UT) with SINFONI (*13*) and on 17 April 2006 UT with OSIRIS. Together the two instruments provide independent measurements of Titan at different epochs and viewing geometries. Systematic errors that arise from mosaicking and correcting for Earth's atmosphere (fig. S1) are specific to each instrument, and comparison facilitates the rejection of observational artifacts. Here we describe a method for making measurements of condensed-phase opacity from specific altitude regions in Titan's atmosphere using narrow (10- to 15-nm) spectral bandpass difference imaging. We used RT models to quantify the altitude and magnitude of the opacity enhancements, and we report the detection of widespread methane drizzle: precipitation from stratiform clouds of solid methane.

In order to discern the light scattered by clouds, drizzle, and haze in the lower troposphere, the contribution from the surface albedo variation (Fig. 1A) was removed from the images that probed the bottom of the atmosphere (Fig. 1B). We empirically quantified the relative surface flux f in images taken at wavelengths with significant and with negligible methane gas opacity by minimizing the correlation coefficient between the surface-subtracted image of the atmosphere and the image of the surface (fig. S2). The mean surface flux in images probing the lower troposphere is ~72% of the flux in images of the surface, which is confirmed by our RT models. After subtracting the surface contribution from images that probe the lower troposphere, we can identify equatorial opacity changes

[1]Department of Astronomy, University of California, Berkeley, CA 94611, USA. [2]Center for Integrative Planetary Science, University of California, Berkeley, CA 94611, USA.

*To whom correspondence should be addressed. E-mail: mate@berkeley.edu

Supporting Online Material for

One-Dimensional Fast Migration of Vacancy Clusters in Metals

Yoshitaka Matsukawa* and Steven J. Zinkle

*To whom correspondence should be addressed. E-mail: ym2@uiuc.edu

Published 9 November 2007, *Science* **318**, 959 (2007)
DOI: 10.1126/science.1148336

This PDF file includes:

Other Supporting Online Material for this manuscript includes the following:
available at www.sciencemag.org/cgi/content/full/318/5852/959/DC1

Materials and Methods

Vacancy clusters were introduced into gold specimens by deformation (Fig. 3) or quenching (Fig. 4) as follows. The starting material for Fig. 3 was a gold ribbon of 99.9975% purity, measuring 10 μm in thickness, and annealed in vacuum at 1173K for 2 h. The gold ribbon was notched in the middle by a razor blade and strained and fractured in a transmission electron microscope (TEM) using a commercial straining stage (GATAN Model 671 single-tilt cooling straining stage) with a crosshead speed of ~1 μm/s at room temperature. Although the gold ribbon was never subjected to any chemical thinning, thin foil regions transparent to a 200-keV electron beam were produced near the fractured edge through thickness reduction accompanied by elongation *(S1)*. The thickness of the thin foil portion was less than 50 nm. A very high density of stacking fault tetrahedron (SFT) and a few vacancy loops were produced together in the remnant thin foil. The vacancy loops exhibited the one-dimensional (1-D) migration as shown in Fig. 3. The TEM observation was carried out at room temperature.

The starting material for Fig. 4 was a gold sheet of 99.9975% purity, measuring 100 μm in thickness. The gold sheet was quenched from 1273K in an open vertical furnace to 233K in a $CaCl_2$ solution. The gold sheet was kept at 1273 K for 10 min in the furnace and at 233 K for 10 min in the quenched-in solution, respectively. After the heat treatment, the sheet was cut into 12.5 mm x 2.5 mm pieces, and then the central portion of the piece was electro-polished using a KCN, 67 g/L solution at room temperature. The gold specimen was mounted on a cooling stage (GATAN Model 671 single-tilt cooling straining stage; however, the specimen was not strained). The microstructure was observed at 113 K about 30 to 60 minutes after the temperature drop to minimize specimen drift associated with thermal gradients.

The motion pictures were captured with a GATAN Model 622 camera at a frame rate of 30 frames/s, recorded on DV tapes, and then computer processed into sequential images.

Conversion mechanism of an SFT from a vacancy-type prismatic loop

Silcox & Hirsch *(S2)*, who first observed SFTs in quenched gold, considered that the characteristic three-dimensional pyramid structure of SFTs was created from a two-dimensional triangular Frank loop via the propagation of Shockley partial dislocations from the loop edges on three crystallographically equivalent {111} planes, as shown in Fig.

S3A. This model is convincing to explain the geometric feature of SFTs, and is reproducible in molecular dynamics (MD) simulations *(S3)*. However, to date no direct observation of this conversion has been reported, though the inverse conversion, i.e. the transformation from an SFT to a triangular Frank loop has been reported by several researchers *(S4-S5)*. If a prismatic vacancy loop transforms to an SFT via this mechanism, the prismatic loop must transform to a triangular Frank loop prior to the Silcox-Hirsch process.

Alternatively, Kuhlmann-Wilsdorf *(S6)* proposed variants of the SFT-loop conversion mechanism, as shown in Fig. S3B-S3D. Her models were originally proposed to explain how an SFT collapsed into a two-dimensional cluster during thermal annealing. The unzipping of a single vertex corresponds to the inverse of the Silcox-Hirsch mechanism, the transformation into a triangular Frank loop. Simultaneous unzipping of multiple vertices results in the transformation into a triangular prismatic loop in either case.

These models imply that the prismatic vacancy loop that exhibited the 1-D motion in Fig. 3 is triangular-shaped as shown in Fig. S4. Note that the vacancy loop examined in the 1999 MD simulations *(S7)* is hexagonal in shape *(S8)*. This is because the stable configuration for prismatic loops in fcc metals is hexagonal for vacancy-type and rhombic for SIA-type in MD simulations *(S9)*. The effect of loop shape on the loop's 1-D motion and the transformation into an SFT needs to be examined further.

Interaction of prismatic loops with gliding dislocations

Although the vacancy loop moved along side the straight dislocation in Fig. 4, the loop clearly kept a certain distance away from it. The straight dislocation has an apparent super jog or kink at the position closest to the moving vacancy loop. As a result of this, the distance is wider (~1 nm) on the upper right portion and narrower (~0.5 nm) on the lower left portion of the dislocation line in Fig. 4. The position of the super jog/kink portion moved together with the moving vacancy loop. In other words, the vacancy loop dragged the super jog/kink.

The straight dislocation was introduced by handling when the thin foil specimen was mounted on the cooling stage. Since the dislocation line is parallel to an edge of an SFT, the character of the straight dislocation is screw or 60 degree. Considering that several investigators have reported screw dislocations are dominant in thin foil deformation on gold

(S2), copper *(S10-S11)*, and nickel *(S12-S13)*, the straight dislocation in Fig. 4 is most likely screw-type *(S14)*.

It is well known that jogs on screw dislocations are obstacles that reduce the mobility of screw dislocations. Since the jogs are edge in character, gliding together with the screw dislocation corresponds to climb motion that requires vacancy absorption. They are glissile 'along' the screw dislocation without vacancy absorption since that is a normal glide direction for the edge segments. However, it is difficult to induce jog motion by a uniform shear stress since a bowed-out screw dislocation interrupts the jog migration path *(S15)*. In Osetsky's MD simulation that reproduced a jog on a screw dislocation in a thin foil condition, the jog migrated toward the foil surface due to the image force from the surface. In the sense that the vacancy loops can transport jogs by the dragging effect, the present results indicate that glissile dislocation loops have the potential to affect the mobility of screw dislocations.

Effect of stress on the 1-D migration

An alternative explanation of the loop's 1-D migration may involve the effect of stress (strain-field) from the other nearby defects or interfaces such as SFTs (Fig. 3), a straight dislocation (Fig. 4), and foil surfaces. In Fig. 3, the strain-field of nearby SFTs certainly affected the 1-D migration. The vacancy loop finally settled down in between two SFTs where the stress on the loop from these two SFTs is balanced: this stress balance may be a significant contributing factor for the self-assembly of SFT arrays. In Fig. 4, the effect of the strain-field of the straight dislocation on the loop 1-D migration is unclear. However, the super-jog on the straight dislocation (most likely an edge segment on the screw dislocation) is immobile without (external shear) stress, whereas the observation was carried out under nominally stress-free conditions. The effect of image force from foil surfaces on the vacancy loop and the super-jog migration was not significant in Fig. 4. The vacancy loop and the jog were originally located near the foil surface at 0 s. The image force from surfaces on a dislocation object is attractive; this would cause the vacancy loop (and also the jog) to migrate toward the nearby surface and annihilate at the surface. However, in our observations the vacancy loop (and the jog) migrated in the opposite direction (i.e. toward the distant surface) at 290 s. Judging from these observations, it is most likely that the loop's 1-D migration was not affected by the image force from foil surfaces and the migration of the dislocation super-jog was induced by the stress-field from

the vacancy loop.

Supporting figures

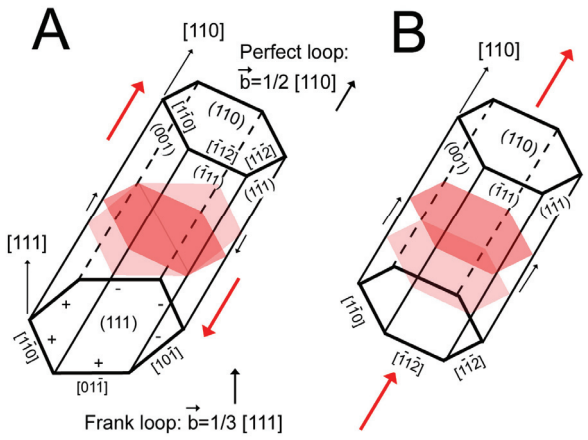

Fig. S1. (A) Shear stress allows dislocation loops to rotate only in the prismatic cylinder. **(B)** In the 1-D migration mode, the entire dislocation loop glides simultaneously in the same direction. The light shaded region represents the original loop habit plane and the dark shaded region represents the location after atomic migration.

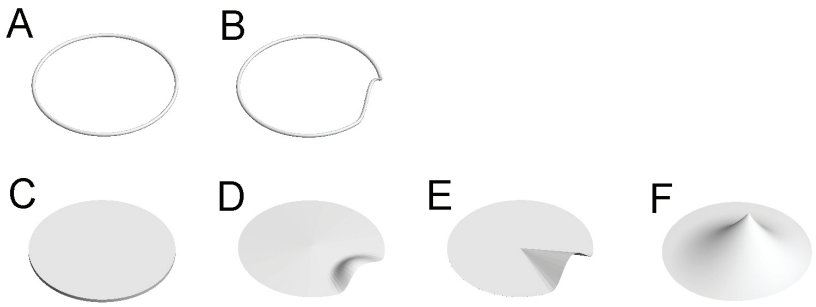

Fig. S2. (A)(B) Double kink in the line tension model: a 2-D step on the dislocation line. **(C)(D)(E)** Double kink considering the 3-D structure, i.e. how propagation of material flow occurs into the loop interior. If the loop motion is induced by double kink mechanism, the materials flow should propagate from the loop perimeter to the center. **(F)** Unlikely manner of material flow from the viewpoint of double kink mechanism.

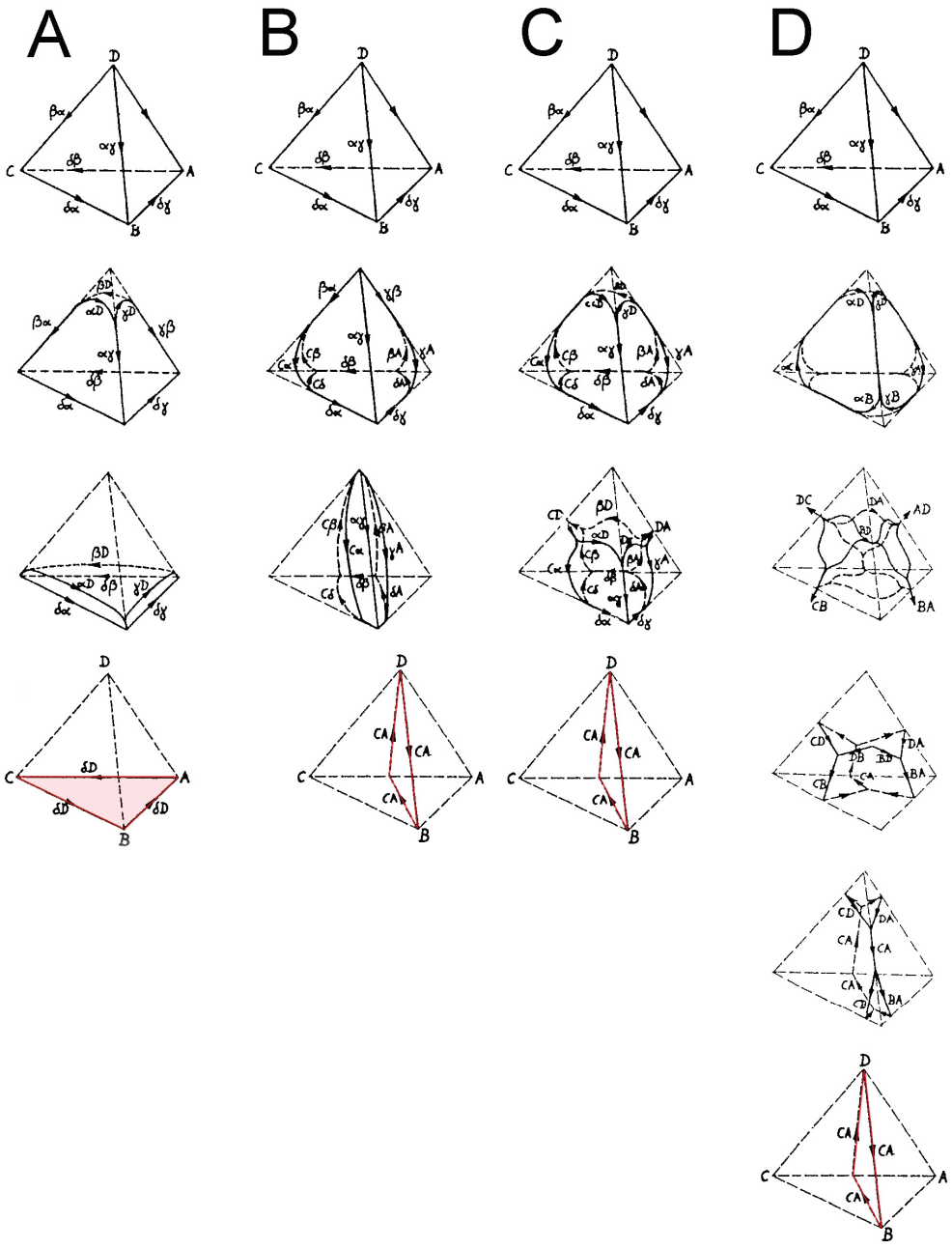

Fig. S3. Collapse processes of an SFT to a dislocation loop proposed by Kuhlmann-Wilsdorf *(S6)*: **(A)** unzipping from a single vertex, **(B)** two vertexes simultaneously, **(C)** three vertexes simultaneously, and **(D)** all four vertexes simultaneously. The resultant 2-D cluster is a triangular Frank loop for **(A)** and a triangular prismatic loop for **(B)(C)(D)**, respectively.

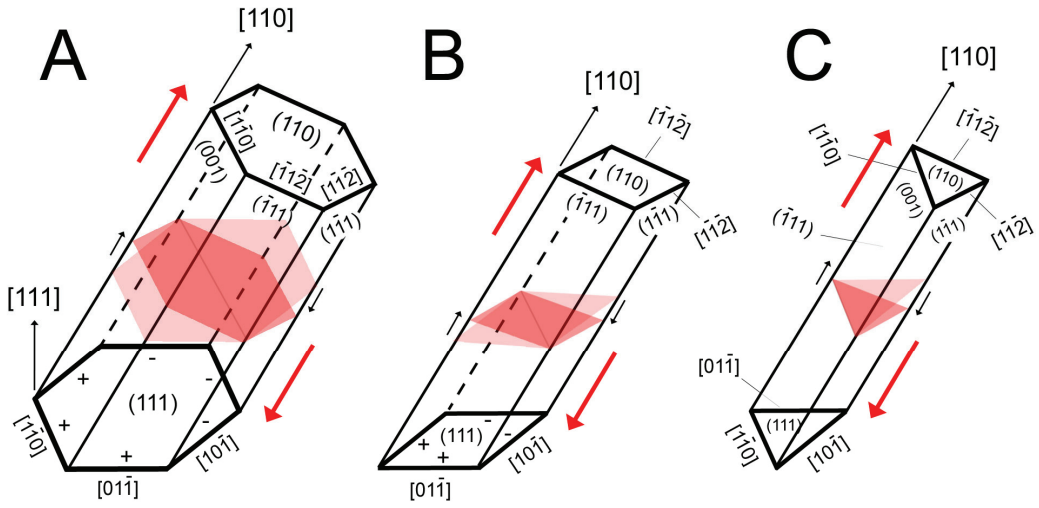

Fig. S4: Various shaped prismatic loops: **(A)** hexagonal, **(B)** rhombic, and **(C)** triangular.

References and Notes

S1. M. Kiritani et al., *Philos. Mag. Lett.* **79** , 797 (1999).

S2. J. Silcox, P. B. Hirsch, *Philos. Mag.* **4**, 72 (1959).

S3. B. D. Wirth, V. Bulatov, T. D. de la Rubia, *J. Nucl. Mater*. **283B**, 773 (2000).

S4. M. J. Yokota, J. Washburn, *Philos. Mag.* **16**, 459 (1967).

S5. Y. Matsukawa, Yu. N. Osetsky, R. E. Stoller, S. J. Zinkle, *J. Nucl. Mater*. **351**, 285 (2006).

S6. D. Kuhlmann-Wilsdorf, *Acta Metall.* **13**, 257 (1965).

S7. Yu. N. Osetsky, D. J. Bacon, A. Serra, *Philos. Mag. Lett.* **79**, 273 (1999).

S8. This information was obtained through personal communication with Yu. N. Osetsky.

S9. M. A. Puigvi, A. Serra, *Philos. Mag. Lett.* **84**, 257 (2004).

S10. J. V. Sharp, *Phil. Mag.* **16**, 77 (1967).

S11. J. S. Robach, I. M. Robertson, B. D. Wirth, and A. Arsenlis, *Phil. Mag.* **83**, 955 (2003).

S12. H. Saka, K. Noda, K. Matsumoto, and T. Imura, *Proceedings of 4th International*

Conference on High Voltage Electron Microscopy, Toulouse, 325 (1975).

S13. K. Noda, H. Saka, K. Shiraishi, H. Yoshida, and T. Imura, *Proceedings of 5th International Conference on High Voltage Electron Microscopy*, Kyoto, 403 (1977).

S14. Since thin foil specimen has less constraint for deformation in the thickness direction (i.e. under so-called 'plane stress' condition), Mode-III out-of-plane shear (tearing) is favored in thin foil deformation. It is well known that screw dislocations compensate the Mode-III out-of-plane shear, in contrast that edge dislocations compensate the Mode-II in-plane shear, which is favored in bulk deformation (under so-called 'plane strain' condition).

S15. Yu. N. Osetsky, R. E. Stoller, Y. Matsukawa, *Philos. Mag. Lett.* **86**, 511 (2006).